

RESEARCH ARTICLE | AUGUST 05 2021

One-stage simplified lattice Boltzmann method for two- and three-dimensional magnetohydrodynamic flows

Special Collection: [Special Issue on the Lattice Boltzmann Method](#)

Alessandro De Rosis   ; Ruizhi Liu (刘睿智)  ; Alistair Revell 

 Check for updates

Physics of Fluids 33, 085114 (2021)

<https://doi.org/10.1063/5.0058884>



View
Online



Export
Citation



Physics of Fluids

Special Topic:
Flow and Climate

Guest Editors: Khaled Ghannam and Mostafa Momen

Submit Today!

 **AIP
Publishing**

One-stage simplified lattice Boltzmann method for two- and three-dimensional magnetohydrodynamic flows

Cite as: Phys. Fluids **33**, 085114 (2021); doi:10.1063/5.0058884

Submitted: 3 June 2021 · Accepted: 22 July 2021 ·

Published Online: 5 August 2021



[View Online](#)



[Export Citation](#)



[CrossMark](#)

Alessandro De Rosis,^{a)} Ruizhi Liu (刘睿智), and Alistair Revell

AFFILIATIONS

Department of Mechanical, Aerospace and Civil Engineering, The University of Manchester, Manchester M13 9PL, United Kingdom

Note: This paper is part of the Special Issue on the Lattice Boltzmann Method.

^{a)}Author to whom correspondence should be addressed: alessandro.derosis@manchester.ac.uk

ABSTRACT

In this paper, we propose a new simplified lattice Boltzmann method (SLBM) for magnetohydrodynamic flows that outperforms the classical one in terms of accuracy, while preserving its advantages. A very recent paper [De Rosis *et al.*, “Double-D2Q9 lattice Boltzmann models with extended equilibrium for two-dimensional magnetohydrodynamic flows,” Phys. Fluids **33**, 035143 (2021)] demonstrated that the SLBM enforces the divergence-free condition of the magnetic field in an excellent manner and involves the lowest amount of virtual memory. However, the SLBM is characterized by the poorest accuracy. Here, the two-stage algorithm that is typical of the SLBM is replaced by a one-stage procedure following the approach devised for non-conductive fluids in a very recent effort [Delgado-Gutierrez *et al.*, “A single-step and simplified graphics processing unit lattice Boltzmann method for high turbulent flows,” Int. J. Numer. Methods Fluids **93**, 2339 (2021)]. The Chapman–Enskog expansion formally demonstrates the consistency of the present scheme. The resultant algorithm is very compact and easily implemented. Given all these features, we believe that the proposed approach is an excellent candidate to perform numerical simulations of two- and three-dimensional magnetohydrodynamic flows.

Published under an exclusive license by AIP Publishing. <https://doi.org/10.1063/5.0058884>

NOMENCLATURE

Abbreviations

BGK	Bhatnagar–Gross–Krook
LBE	Lattice Boltzmann equation
LBM	Lattice Boltzmann method
MRT	Multiple-relaxation time
SLBM	Two-stage simplified lattice Boltzmann method
SSLBM	One-stage simplified lattice Boltzmann method

Dimensionless numbers

Ma	Mach number
Pr _m	Magnetic Prandtl number
Re	Reynolds number

Superscripts

† Quantity computed at the predictor stage

Subscripts

i Index spanning the lattice directions

Symbols

B	Magnetic field vector
<i>c</i> _s	Lattice sound speed
c _{<i>i</i>}	Lattice directions
<i>E</i>	Total energy
<i>E</i> _m	Magnetic energy
<i>E</i> _k	Kinetic energy
<i>f</i> _{<i>i</i>} ^{eq}	Equilibrium distributions for the velocity field
<i>g</i> _{<i>i</i>} ^{eq}	Equilibrium distributions for the magnetic field
j	Density of the electric current vector
m	Fluid momentum vector
ε	Dissipation rate
u	Velocity vector
<i>t</i>	Time

w_i	Weighting factors
Δ	Laplacian operator
∇	Spatial derivative operator
ν	Kinematic viscosity
ρ	Density
ζ	Vorticity vector
τ_ν, τ_η	Relaxation times

I. INTRODUCTION

The investigation of the behavior of electrically conducting fluids, also known as magnetohydrodynamics (MHD), is nowadays an important topic in contemporary computational fluid dynamics.¹ Indeed, its area of employment is impressively wide. The design of electromagnetic pumps^{2,3} and cooling systems for nuclear reactors,⁴ the predictions of solar flares,^{5,6} the measurement of flow velocities in hot and aggressive liquids,^{7,8} and drop-on-demand printability⁹ are just few compelling examples of the most challenging applications of MHD.

From a mathematical viewpoint, the flow of an electrically conductive fluid is governed by the magnetic induction equation

$$\partial_t \mathbf{B} = \nabla \times (\mathbf{u} \times \mathbf{B}) + \eta \Delta \mathbf{B}, \quad (1)$$

where t is the time, η is the magnetic diffusivity, and \mathbf{u} and \mathbf{B} are the velocity and magnetic field vectors, respectively, accompanied by the divergence-free condition

$$\nabla \cdot \mathbf{B} = 0, \quad (2)$$

together with the incompressible Navier–Stokes equations for MHD, that is,

$$\partial_t \mathbf{u} + (\mathbf{u} \cdot \nabla) \mathbf{u} = -\frac{\nabla p}{\rho} + \nu \Delta \mathbf{u} + \frac{\mathbf{j} \times \mathbf{B}}{\rho}, \quad (3)$$

$$\nabla \cdot \mathbf{u} = 0, \quad (4)$$

where ρ is the mass density, p is the pressure, ν is the fluid kinematic viscosity, and $\mathbf{j} = \nabla \times \mathbf{B}$ is the density of electric current vector.

A closed-form solution of this set of equations is available only in few cases, where the flow and the geometry undergo significant simplifications. The most popular example is the simple (laminar) Hartmann flow, where an electrically conductive fluid flows between two parallel plates with an external magnetic field being perpendicular to the channel walls.¹⁰ Unfortunately, the aforementioned practical applications involve complex (turbulent) flows and geometries. Therefore, the usage of numerical methods is essential. Spectral and pseudo-spectral methods represent a very well-consolidated approach to MHD problems.^{11–16} However, the capability to accurately simulate flows in complex geometries with possibly moving parts is one of the key current issues in computational MHD.

An alternative to classical macroscopic-based approaches can be found in the mesoscopic-based lattice Boltzmann method (LBM).^{17–19} In the LBM, the flow is idealized by collections (also known as populations or distributions) of fictitious particles, colliding and streaming along the links of a Cartesian lattice that is kept fixed through the whole analysis. Before going any further, let us highlight that fluid dynamics stems from the computation of the evolution of populations. Despite the algorithmic simplicity of the resultant algorithm, it should

be noted that it might lead to a very large memory usage, especially when running three-dimensional simulations, due to the storage of the particle distribution functions at each lattice node. Interestingly, the simplified lattice Boltzmann method^{20–27} (SLBM) avoids the computation of the space–time evolution of the particle distribution functions, as it involves only macroscopic variables. Hence, the SLBM demands to compute and store only these quantities at each lattice site, while the computation and storage of populations are completely neglected. As a consequence, the amount of involved virtual memory is drastically reduced.

The earliest attempts to demonstrate the suitability of the LBM to simulate MHD flows were carried out by Succi *et al.*,²⁸ Chen *et al.*,²⁹ and Martínez *et al.*³⁰ Later, Dellar³¹ proposed a seminal contribution, where the physics of an electrically conductive fluid is governed by two sets of populations: a scalar one retaining the fluid flow and a vector-valued one recovering the solution of the magnetic induction equation. Despite the very accurate predictions performed by this approach, De Rosis *et al.*³² demonstrated that it is unsuitable when the magnetohydrodynamic flows are turbulent. This behavior must be addressed to the disadvantages of the Bhatnagar–Gross–Krook (BGK) collision operator,³³ that is, the one adopted by Dellar.³¹ Indeed, the intrinsic unavoidable presence of non-hydrodynamic ghost modes, which undermine the stability of the algorithm through spurious couplings with hydrodynamic ones,^{34–38} accompanied by the common practice to relax populations to an incomplete local equilibrium,^{39–48} promotes a sudden blow-up of the BGK-based simulations when the fluid kinematic viscosity reduces.

In a very recent paper, De Rosis *et al.*⁴⁹ have performed a comprehensive comparison of four different LBMs for MHD: (i) the BGK LBM, the multiple-relaxation-time (MRT) LBMs based on (ii) raw and (iii) central moments (CMS), and (iv) the simplified lattice Boltzmann method. From the reported extensive analysis, two main results have been found. First, the adoption of the D2Q9 discretization for the populations addressing the evolution of \mathbf{B} instead of the D2Q5 one (as suggested by Dellar³¹) is instrumental to achieve more accurate computations. Second, the divergence-free condition of the magnetic field (which should be ensured by any scheme for MHD flows^{50–54}) is enforced in an excellent manner only by the SLBM, which shows results very close to the round-off error. However, the SLBM shows the lowest accuracy, and this is particularly emphasized when coarse grid resolutions are adopted.⁴⁹ This should be addressed to its level of numerical dissipation that is generally higher than the one obtained by the BGK or MRT LBMs.⁵⁵

In this work, we present a new simplified scheme for magnetohydrodynamic flows. Instead of using the classical two-stage predictor–corrector technique, we develop a one-stage lattice Boltzmann method (SSLBM). While keeping the same excellent properties on the satisfaction of the divergence-free condition, our proposed strategy exhibits a superior accuracy, that is, particularly evident in three-dimensional scenarios. The resultant procedure is very compact and easy to be implemented.

The rest of the paper is organized as follows. In Sec. II, the numerical methodology is devised. Results from two- and three-dimensional analyses are discussed in Sec. III. Eventually, some conclusions are drawn in Sec. IV.

II. LATTICE BOLTZMANN METHOD

In this section, first the simplified LBM by De Rosis *et al.*⁴⁹ is recalled. Second, our one-stage simplified LBM for two-dimensional

magnetohydrodynamic flows is devised. Eventually, we demonstrate that its extension to three dimensions is straightforward and its algorithm is outlined.

A. Two-dimensional two-stage simplified LBM by De Rosis et al.⁴⁹

Let us consider a two-dimensional Cartesian space $\mathbf{x} = [x, y]$ and the D2Q9 velocity discretization, where lattice directions are $\mathbf{c}_i = [c_{ix}, c_{iy}]$ with

$$c_{ix} = [0, 1, 0, -1, 0, 1, -1, -1, 1], \quad (5)$$

$$c_{iy} = [0, 0, 1, 0, -1, 1, 1, -1, -1]. \quad (6)$$

In two dimensions, the velocity and magnetic field vectors have two components, that is, $\mathbf{u} = [u_x, u_y]$, $\mathbf{B} = [B_x, B_y]$. Conversely, the density of electric current and the vorticity possess only one component, that is, $j = [j]$ and $\zeta = [\zeta]$. Let us also introduce the vector of the fluid momentum $\mathbf{m} = \rho\mathbf{u} = [m_x, m_y]$.

Given the solution at the time t , the classical simplified LBM involves a two-stage fractional step technique, that is,

Predictor step:

$$\begin{aligned} \rho^\dagger(\mathbf{x}, t + \Delta t) &= \sum_i f_i^{eq}(\mathbf{x} - \mathbf{c}_i \Delta t, t), \\ \mathbf{m}^\dagger(\mathbf{x}, t + \Delta t) &= \sum_i \mathbf{c}_i f_i^{eq}(\mathbf{x} - \mathbf{c}_i \Delta t, t), \\ \mathbf{B}^\dagger(\mathbf{x}, t + \Delta t) &= \sum_i \mathbf{g}_i^{eq}(\mathbf{x} - \mathbf{c}_i \Delta t, t), \end{aligned} \quad (7)$$

where the superscript \dagger denotes predicted (intermediate) quantities, and

Corrector step:

$$\begin{aligned} \rho(\mathbf{x}, t + \Delta t) &= \rho^\dagger(\mathbf{x}, t + \Delta t), \\ \mathbf{m}(\mathbf{x}, t + \Delta t) &= \mathbf{m}^\dagger(\mathbf{x}, t + \Delta t) + (\tau_\nu - 1) \\ &\quad \times \sum_i \mathbf{c}_i f_i^{eq,\dagger}(\mathbf{x} + \mathbf{c}_i \Delta t, t + \Delta t) - (\tau_\nu - 1) \mathbf{m}(\mathbf{x}, t), \\ \mathbf{B}(\mathbf{x}, t + \Delta t) &= \mathbf{B}^\dagger(\mathbf{x}, t + \Delta t) + (\tau_\eta - 1) \\ &\quad \times \sum_i \mathbf{g}_i^{eq,\dagger}(\mathbf{x} + \mathbf{c}_i \Delta t, t + \Delta t) - (\tau_\eta - 1) \mathbf{B}(\mathbf{x}, t). \end{aligned} \quad (8)$$

The two relaxation times, τ_ν and τ_η , are linked to the fluid kinematic viscosity and magnetic diffusivity as

$$\nu = \left(\tau_\nu - \frac{1}{2} \right) c_s^2, \quad (9)$$

$$\eta = \left(\tau_\eta - \frac{1}{2} \right) c_s^2, \quad (10)$$

respectively.³¹ Within the framework of the one-stage and two-stage simplified LBM, equilibrium populations are usually written by a second-order truncated expression. Here, f_i^{eq} is computed by expanding onto the full basis of Hermite polynomials (up to the fourth order) according to De Rosis *et al.*,⁴⁹ that is,

$$\begin{aligned} f_i^{eq} &= w_i \rho \left[1 + \frac{\mathcal{H}_i^{(1)} \cdot \mathbf{u}}{c_s^2} + \frac{1}{2c_s^4} \mathcal{H}_i^{(2)} : \mathbf{u}\mathbf{u} \right. \\ &\quad \left. + \frac{1}{2c_s^6} \left(\mathcal{H}_{ixxy}^{(3)} u_x^2 u_y + \mathcal{H}_{ixyy}^{(3)} u_x u_y^2 \right) \right. \\ &\quad \left. + \frac{1}{4c_s^8} \mathcal{H}_{ixxyy}^{(4)} u_x^2 u_y^2 \right] + \frac{w_i}{2c_s^4} \left[\frac{1}{2} |\mathbf{c}_i|^2 |\mathbf{B}|^2 - (\mathbf{c}_i \cdot \mathbf{B})^2 \right], \end{aligned} \quad (11)$$

$$g_{ix}^{eq} = w_i \left[B_x + \frac{c_{iy}}{c_s^2} (u_y B_x - u_x B_y) \right], \quad (12)$$

$$g_{iy}^{eq} = w_i \left[B_y + \frac{c_{ix}}{c_s^2} (u_x B_y - u_y B_x) \right], \quad (13)$$

where $\mathbf{g}_i^{eq} = [g_{ix}^{eq}, g_{iy}^{eq}]$, the weights are $w_0 = 4/9$, $w_{1\dots 4} = 1/9$, $w_{5\dots 8} = 1/36$, the lattice sound speed is $c_s = 1/\sqrt{3}$, and Hermite polynomials are

$$\begin{aligned} \mathcal{H}_{ix}^{(1)} &= c_{ix}, \\ \mathcal{H}_{iy}^{(1)} &= c_{iy}, \\ \mathcal{H}_{ixx}^{(2)} &= c_{ix}^2 - c_s^2, \\ \mathcal{H}_{iyy}^{(2)} &= c_{iy}^2 - c_s^2, \\ \mathcal{H}_{ixy}^{(2)} &= c_{ix} c_{iy}, \\ \mathcal{H}_{ixxy}^{(3)} &= (c_{ix}^2 - c_s^2) c_{iy}, \\ \mathcal{H}_{ixyy}^{(3)} &= (c_{iy}^2 - c_s^2) c_{ix}, \\ \mathcal{H}_{ixxyy}^{(4)} &= (c_{ix}^2 - c_s^2) (c_{iy}^2 - c_s^2). \end{aligned} \quad (14)$$

Notice that the equilibrium states $f_i^{eq,\dagger}$ and $\mathbf{g}_i^{eq,\dagger}$ are computed by adopting the predicted values, that is, $f_i^{eq,\dagger} = f_i^{eq}(\rho^\dagger, \mathbf{u}^\dagger, \mathbf{B}^\dagger)$ and $\mathbf{g}_i^{eq,\dagger} = \mathbf{g}_i^{eq}(\mathbf{u}^\dagger, \mathbf{B}^\dagger)$.

B. Two-dimensional one-stage simplified LBM

More recently, Delgado-Gutierrez *et al.*⁵⁶ proposed a one-stage simplified lattice Boltzmann method, where the two-stage predictor–corrector strategy is replaced by an algorithm spanning the lattice point just once per time step. We now derive an SSLBM for MHD flows.

For simplicity, let us just consider one of the particle distribution functions, g_{ix} . The lattice Boltzmann equation (LBE) can be written as

$$g_{ix}(\mathbf{x} + \mathbf{c}_i \Delta t, t + \Delta t) - g_{ix}(\mathbf{x}, t) = \frac{g_{ix}^{eq}(\mathbf{x}, t) - g_{ix}(\mathbf{x}, t)}{\tau_\eta}. \quad (15)$$

By applying a Taylor series expansion at the left-hand side of Eq. (15) followed by a Chapman–Enskog analysis, it is possible to write the following equations:

$$\frac{g_{ix}^{(0)} - g_{ix}^{eq}}{\tau_\eta \Delta t} = 0, \quad (16)$$

$$\Delta g_{ix}^{(0)} + \frac{g_{ix}^{(1)}}{\tau_\eta \Delta t} = 0, \quad (17)$$

$$\frac{\partial g_{ix}^{(0)}}{\partial t_1} + \left(1 - \frac{1}{2\tau_\eta} \right) \Delta g_{ix}^{(1)} = 0. \quad (18)$$

From Eqs. (16) and (17), we obtain

$$g_{ix}^{(0)} = g_{ix}^{eq}, \quad (19)$$

$$g_{ix}^{(1)} \equiv g_{ix}^{neq} = -\tau_\eta \Delta t \Delta g_{ix}^{eq}. \quad (20)$$

Following the SLBM, it is possible to get:

$$g_{ix}^{neq}(\mathbf{x}, t) = -\tau_\eta [g_{ix}^{eq}(\mathbf{x}, t) - g_{ix}^{eq}(\mathbf{x} - \mathbf{c}_i \Delta t, t - \Delta t)]. \quad (21)$$

We can further write

$$\frac{\partial g_{ix}^{(0)}}{\partial t_0} = -\mathbf{c}_i \cdot \nabla g_{ix}^{(0)}, \quad (22)$$

$$\frac{\partial g_{ix}^{(1)}}{\partial t_0} = -\left(1 - \frac{1}{2\tau_\eta}\right) \Delta g_{ix}^{(1)}. \quad (23)$$

By combining these two equations, we have

$$\frac{\partial g_{ix}^{(0)}}{\partial t} = -\mathbf{c}_i \cdot \nabla g_{ix}^{(0)} - \left(1 - \frac{1}{2\tau_\eta}\right) \Delta g_{ix}^{(1)}. \quad (24)$$

Let us sum the above equation over the lattice directions, that is,

$$\sum_i \left[\frac{\partial g_{ix}^{(0)}}{\partial t} + \mathbf{c}_i \cdot \nabla g_{ix}^{(0)} + \left(1 - \frac{1}{2\tau_\eta}\right) \Delta g_{ix}^{(1)} \right] = 0. \quad (25)$$

Interestingly, it is possible to write

$$\frac{\partial g_{ix}^{(0)}}{\partial t} = g_{ix}^{(0)}(\mathbf{x}, t + \Delta t) - g_{ix}^{(0)}(\mathbf{x}, t), \quad (26)$$

$$\mathbf{c}_i \cdot \nabla g_{ix}^{(0)} = \frac{g_{ix}^{(0)}(\mathbf{x} + \mathbf{c}_i \Delta t, t) - g_{ix}^{(0)}(\mathbf{x} - \mathbf{c}_i \Delta t, t)}{2}, \quad (27)$$

$$\begin{aligned} \Delta g_{ix}^{(1)} &= \frac{\partial}{\partial t_0} g_{ix}^{(1)} + \mathbf{c}_i \cdot \nabla g_{ix}^{(1)} \cong \frac{\partial g_{ix}^{(1)}}{\partial \mathbf{c}_i} = \frac{g_{ix}^{(1)}(\mathbf{x} + \mathbf{c}_i \Delta t, t) - g_{ix}^{(1)}(\mathbf{x}, t)}{\partial \mathbf{c}_i} \\ &= -\tau_\eta \left[g_{ix}^{(0)}(\mathbf{x} + \mathbf{c}_i \Delta t, t) - 2g_{ix}^{(0)}(\mathbf{x}, t) + g_{ix}^{(0)}(\mathbf{x} - \mathbf{c}_i \Delta t, t) \right]. \end{aligned} \quad (28)$$

Then, we get

$$\begin{aligned} \sum_i \left[g_{ix}^{(0)}(\mathbf{x}, t + \Delta t) + 2(\tau_\eta - 1)g_{ix}^{(0)}(\mathbf{x}, t) \right. \\ \left. - (\tau_\eta - 1)g_{ix}^{(0)}(\mathbf{x} + \mathbf{c}_i \Delta t, t) - \tau_\eta g_{ix}^{(0)}(\mathbf{x} - \mathbf{c}_i \Delta t, t) \right] = 0. \end{aligned} \quad (29)$$

By noticing that

$$\begin{aligned} \sum_i g_{ix}^{(0)}(\mathbf{x}, t + \Delta t) &= B_x(\mathbf{x}, t + \Delta t), \\ \sum_i g_{ix}^{(0)}(\mathbf{x}, t) &= B_x(\mathbf{x}, t), \end{aligned} \quad (30)$$

and by introducing

$$\begin{aligned} B_{xf} &= \sum_i g_{ix}^{(0)}(\mathbf{x} + \mathbf{c}_i \Delta t, t), \\ B_{xb} &= \sum_i g_{ix}^{(0)}(\mathbf{x} - \mathbf{c}_i \Delta t, t), \\ B_{xc} &= \sum_i g_{ix}^{(0)}(\mathbf{x}, t) = B_x(\mathbf{x}, t), \end{aligned} \quad (31)$$

we end up with

$$B_x(\mathbf{x}, t + \Delta t) = B_{xb} + (\tau_\eta - 1)(B_{xf} - 2B_{xc} + B_{xb}). \quad (32)$$

Having achieved this result, we are now in the position to deploy the one-stage simplified lattice Boltzmann method as follows:

$$\begin{aligned} \rho(\mathbf{x}, t + \Delta t) &= \frac{1}{2} \rho_f - \rho_c + \frac{3}{2} \rho_b, \\ \mathbf{m}(\mathbf{x}, t + \Delta t) &= \mathbf{m}_b + (\tau_\nu - 1)(\mathbf{m}_f - 2\mathbf{m}_c + \mathbf{m}_b), \\ \mathbf{B}(\mathbf{x}, t + \Delta t) &= \mathbf{B}_b + (\tau_\eta - 1)(\mathbf{B}_f - 2\mathbf{B}_c + \mathbf{B}_b), \end{aligned} \quad (33)$$

where,

$$\begin{aligned} \rho_f &= \sum_i f_i^{eq}(\mathbf{x} + \mathbf{c}_i \Delta t, t), \\ \rho_b &= \sum_i f_i^{eq}(\mathbf{x} - \mathbf{c}_i \Delta t, t), \\ \rho_c &= \rho(\mathbf{x}, t), \\ \mathbf{m}_f &= \sum_i f_i^{eq}(\mathbf{x} + \mathbf{c}_i \Delta t, t) \mathbf{c}_i, \\ \mathbf{m}_b &= \sum_i f_i^{eq}(\mathbf{x} - \mathbf{c}_i \Delta t, t) \mathbf{c}_i, \\ \mathbf{m}_c &= \rho(\mathbf{x}, t) \mathbf{u}(\mathbf{x}, t), \\ \mathbf{B}_f &= \sum_i \mathbf{g}_i^{eq}(\mathbf{x} + \mathbf{c}_i \Delta t, t), \\ \mathbf{B}_b &= \sum_i \mathbf{g}_i^{eq}(\mathbf{x} - \mathbf{c}_i \Delta t, t), \\ \mathbf{B}_c &= \mathbf{B}(\mathbf{x}, t). \end{aligned} \quad (34)$$

Eventually, the fluid velocity can then be simply computed as

$$\mathbf{u}(\mathbf{x}, t + \Delta t) = \frac{\mathbf{m}(\mathbf{x}, t + \Delta t)}{\rho(\mathbf{x}, t + \Delta t)}. \quad (35)$$

Equations (33)–(35), accompanied by the expressions of the equilibrium populations in Eqs. (11)–(13), represent the core of the algorithm of the proposed SSLBM.

Let us underline that the present (one-stage) SSLBM retains the salient advantages of the (two-stage) SLBM. First, the computation of the evolution of the particle distribution functions is completely avoided. Overall, it demands to store an amount of information that is 5.4 times lower than the virtual memory requested by the LBMs with the evolution of populations (BGK and MRT). This is even more emphasized in three dimensions, where the D3Q19 and D3Q27 discretizations could be used. In these cases, the amounts of information to be saved are 9.8 and 15.6 times lower, respectively.⁴⁹ Second, boundary conditions just consist of assigning the desired values of the macroscopic variables, without involving any particular (populations-based) treatment and additional implementation.

C. Extension to three dimensions of the one-stage simplified LBM

In three dimensions, let us consider a two-dimensional Cartesian space $\mathbf{x} = [x, y, z]$ and the D3Q19 velocity discretization, where lattice directions are $\mathbf{c}_i = [c_{ix}, c_{iy}, c_{iz}]$ with

$$\begin{aligned} c_{ix} &= [0, 1, -1, 0, 0, 0, 1, -1, 1, -1, 1, -1, 0, 0, 0, 0], \\ c_{iy} &= [0, 0, 0, 1, -1, 0, 0, 1, -1, -1, 1, 0, 0, 0, 1, -1, 1, -1], \quad (36) \\ c_{iz} &= [0, 0, 0, 0, 0, 1, -1, 0, 0, 0, 0, 1, -1, -1, 1, 1, -1, 1]. \end{aligned}$$

In this case, the velocity, magnetic field and density of electric current, and vorticity vectors have three components, that is, $\mathbf{u} = [u_x, u_y, u_z]$, $\mathbf{B} = [B_x, B_y, B_z]$, $\mathbf{j} = [j_x, j_y, j_z]$, and $\boldsymbol{\zeta} = [\zeta_x, \zeta_y, \zeta_z]$. The fluid momentum is $\mathbf{m} = [m_x, m_y, m_z]$.

Coreixas *et al.*⁵⁷ proposed a derivation of the equilibrium that is compliant with all collision models, and the corresponding expressions are

$$\begin{aligned} f_{(0,0,0)}^{eq} &= \frac{\rho}{3} \left[1 - (u_x^2 + u_y^2 + u_z^2) + 3(u_x^2 u_y^2 + u_x^2 u_z^2 + u_y^2 u_z^2) \right], \\ f_{(\sigma,0,0)}^{eq} &= \frac{\rho}{18} \left[1 + 3\sigma u_x + 3(u_x^2 - u_y^2 - u_z^2) \right. \\ &\quad \left. - 9\sigma(u_x u_y^2 + u_x u_z^2) - 9(u_x^2 u_y^2 + u_x^2 u_z^2) \right], \\ f_{(0,\lambda,0)}^{eq} &= \frac{\rho}{18} \left[1 + 3\lambda u_y + 3(-u_x^2 + u_y^2 - u_z^2) \right. \\ &\quad \left. - 9\lambda(u_x^2 u_y + u_y u_z^2) - 9(u_x^2 u_y^2 + u_y^2 u_z^2) \right], \\ f_{(0,0,\chi)}^{eq} &= \frac{\rho}{18} \left[1 + 3\chi u_z + 3(-u_x^2 - u_y^2 + u_z^2) \right. \\ &\quad \left. - 9\chi(u_x^2 u_z + u_y u_z^2) - 9(u_x^2 u_z^2 + u_y^2 u_z^2) \right], \quad (37) \\ f_{(\sigma,\lambda,0)}^{eq} &= \frac{\rho}{36} \left[1 + 3(\sigma u_x + \lambda u_y) + 3(u_x^2 + u_y^2) \right. \\ &\quad \left. + 9\sigma\lambda u_x u_y + 9(\lambda u_x^2 u_y + \sigma u_x u_y^2) + 9u_x^2 u_y^2 \right], \\ f_{(\sigma,0,\chi)}^{eq} &= \frac{\rho}{36} \left[1 + 3(\sigma u_x + \chi u_z) + 3(u_x^2 + u_z^2) \right. \\ &\quad \left. + 9\sigma\chi u_x u_z + 9(\chi u_x^2 u_z + \sigma u_x u_z^2) + 9u_x^2 u_z^2 \right], \\ f_{(0,\lambda,\chi)}^{eq} &= \frac{\rho}{36} \left[1 + 3(\lambda u_y + \chi u_z) + 3(u_y^2 + u_z^2) \right. \\ &\quad \left. + 9\lambda\chi u_y u_z + 9(\chi u_y^2 u_z + \lambda u_y u_z^2) + 9u_y^2 u_z^2 \right], \end{aligned}$$

where, for the sake of compactness, the tensor product notation has been adopted⁵⁸ with $(\sigma, \gamma, \chi) \in \{\pm 1\}^3$ are three indices assuming the same value of the components of the lattice directions vectors. These expressions are then corrected by adding the term

$$\frac{w_i}{2c_s^4} \left[\frac{1}{3} |\mathbf{c}_i|^2 |\mathbf{B}|^2 - (\mathbf{c}_i \cdot \mathbf{B})^2 \right], \quad (38)$$

where the weights are $w_0 = 1/3$, $w_{1,\dots,6} = 1/18$, and $w_{7,\dots,18} = 1/36$. The equilibrium populations of the magnetic field are $\mathbf{g}_i^{eq} = [g_{ix}^{eq}, g_{iy}^{eq}, g_{iz}^{eq}]$, which assume the following form:

$$g_{ix}^{eq} = w_i \left[B_x + \frac{c_{iy}}{c_s^2} (u_y B_x - u_x B_y) + \frac{c_{iz}}{c_s^2} (u_z B_x - u_x B_z) \right], \quad (39)$$

$$g_{iy}^{eq} = w_i \left[B_y + \frac{c_{ix}}{c_s^2} (u_x B_y - u_y B_x) + \frac{c_{iz}}{c_s^2} (u_z B_y - u_y B_z) \right], \quad (40)$$

$$g_{iz}^{eq} = w_i \left[B_z + \frac{c_{ix}}{c_s^2} (u_x B_z - u_z B_x) + \frac{c_{iy}}{c_s^2} (u_y B_z - u_z B_y) \right]. \quad (41)$$

By simply changing the equilibrium populations and the lattice directions, we are immediately in the position to solve Eqs. (33)–(35) to run a three-dimensional simulation without any additional change.

For the sake of completeness, let us just mention that this three-dimensional model can be adapted straightforwardly to the D3Q27 lattice discretization by simply changing the lattice directions as

$$\begin{aligned} c_{ix} &= [0, 1, -1, 0, 0, 0, 1, -1, 1, -1, 1, -1, 1, -1, \\ &\quad 0, 0, 0, 1, -1, 1, -1, 1, -1, 1, -1], \\ c_{iy} &= [0, 0, 0, 1, -1, 0, 0, 1, 1, -1, -1, 0, 0, 0, 1, \\ &\quad -1, 1, -1, 1, 1, -1, 1, 1, -1, 1, -1], \\ c_{iz} &= [0, 0, 0, 0, 0, 1, -1, 0, 0, 0, 1, 1, 1, -1, 1, 1, \\ &\quad -1, -1, 1, 1, 1, -1, -1, -1, 1], \end{aligned} \quad (42)$$

and by expanding the equilibrium distribution onto the complete basis composed of 27 Hermite polynomials

$$\begin{aligned} f_i^{eq} &= w_i \rho \left\{ 1 + \frac{\mathbf{c}_i \cdot \mathbf{u}}{c_s^2} + \frac{1}{2c_s^4} \left[\mathcal{H}_{ixx}^{(2)} u_x^2 + \mathcal{H}_{iyy}^{(2)} u_y^2 + \mathcal{H}_{izz}^{(2)} u_z^2 \right. \right. \\ &\quad \left. \left. + 2 \left(\mathcal{H}_{ixy}^{(2)} u_x u_y + \mathcal{H}_{ixz}^{(2)} u_x u_z + \mathcal{H}_{iyz}^{(2)} u_y u_z \right) \right] \right. \\ &\quad \left. + \frac{1}{2c_s^6} \left[\mathcal{H}_{ixxy}^{(3)} u_x^2 u_y + \mathcal{H}_{ixxz}^{(3)} u_x^2 u_z + \mathcal{H}_{iyyz}^{(3)} u_x u_y^2 \right. \right. \\ &\quad \left. \left. + \mathcal{H}_{ixzz}^{(3)} u_x u_z^2 + \mathcal{H}_{ijyz}^{(3)} u_y u_z^2 + \mathcal{H}_{ijyz}^{(3)} u_y^2 u_z + 2 \mathcal{H}_{ixyz}^{(3)} u_x u_y u_z \right] \right. \\ &\quad \left. + \frac{1}{4c_s^8} \left[\mathcal{H}_{ixxyy}^{(4)} u_x^2 u_y^2 + \mathcal{H}_{ixxzz}^{(4)} u_x^2 u_z^2 + \mathcal{H}_{iyyzz}^{(4)} u_y^2 u_z^2 \right. \right. \\ &\quad \left. \left. + 2 \left(\mathcal{H}_{ixyzz}^{(4)} u_x u_y u_z^2 + \mathcal{H}_{ixyyz}^{(4)} u_x u_y^2 u_z + \mathcal{H}_{ixxyz}^{(4)} u_x^2 u_y u_z \right) \right] \right. \\ &\quad \left. + \frac{1}{4c_s^{10}} \left[\mathcal{H}_{ixxyzz}^{(5)} u_x^2 u_y u_z^2 + \mathcal{H}_{ixxyyz}^{(5)} u_x^2 u_y^2 u_z + \mathcal{H}_{ixyyzz}^{(5)} u_x u_y^2 u_z^2 \right. \right. \\ &\quad \left. \left. + \frac{1}{8c_s^{12}} \mathcal{H}_{ixxyyzz}^{(6)} u_x^2 u_y^2 u_z^2 \right] \right\} + \frac{w_i}{2c_s^4} \left[\frac{1}{3} |\mathbf{c}_i|^2 |\mathbf{B}|^2 - (\mathbf{c}_i \cdot \mathbf{B})^2 \right], \quad (43) \end{aligned}$$

where the weights are $w_0 = 8/27$, $w_{1,\dots,6} = 2/27$, $w_{7,\dots,18} = 1/54$, and $w_{19,\dots,26} = 1/216$. $\mathcal{H}_i^{(n)}$ denotes the n th-order Hermite polynomial tensor. Coefficients before these tensors are $(n_x! n_y! n_z!) c_s^{2n}$ ⁻¹, where n_x , n_y , and n_z are the number of occurrences of x , y , and z , respectively.⁴⁴

III. RESULTS AND DISCUSSION

In this section, we report the results of simulations in two and three dimensions.

A. Two-dimensional simulations

Here, the accuracy of the above-outlined one-stage simplified lattice Boltzmann method is tested against the numerical predictions of the two-dimensional Orszag–Tang vortex problem¹¹ by De Rosis *et al.*⁴⁹ obtained by four different LBMs: (i) the one-relaxation-time LBM (BGK), the multiple-relaxation-time LBM based on the relaxation of (ii) raw (MRT) and (iii) central moments (CMS), and (iv) the two-stage simplified LBM.

Let us consider a doubly periodic domain of size $A = 2\pi \times 2\pi$. The velocity and magnetic fields are initialized as

$$\begin{aligned} \mathbf{u}(\mathbf{x}, t=0) &= u_0[-\sin y, \sin x], \\ \mathbf{B}(\mathbf{x}, t=0) &= b_0[-\sin y, \sin 2x]. \end{aligned} \quad (44)$$

where $u_0 = b_0 = 2$. The density is initially set equal to 1 everywhere. The kinetic and magnetic energies averaged by the domain size are

$$E_k = \frac{1}{2A} \sum_x \rho(\mathbf{x}) |\mathbf{u}(\mathbf{x})|^2, \quad E_m = \frac{1}{2A} \sum_x |\mathbf{B}(\mathbf{x})|^2, \quad (45)$$

respectively. The total energy is $E = E_k + E_m$. The kinetic and magnetic enstrophies averaged by the domain size are

$$\Omega_k = \frac{1}{2A} \sum_x \zeta(\mathbf{x})^2, \quad \Omega_m = \frac{1}{2A} \sum_x j(\mathbf{x})^2, \quad (46)$$

where

$$\zeta(\mathbf{x}) = \nabla \times \mathbf{u}(\mathbf{x}) = \partial_y u_x(\mathbf{x}) - \partial_x u_y(\mathbf{x}), \quad (47)$$

$$j(\mathbf{x}) = \nabla \times \mathbf{B}(\mathbf{x}) = \partial_y B_x(\mathbf{x}) - \partial_x B_y(\mathbf{x}) \quad (48)$$

are the vorticity and the density of electric current, respectively. The dissipation rate is

$$\epsilon = \nu \Omega_k + \eta \Omega_m. \quad (49)$$

The divergence of the magnetic field is

$$\nabla \cdot \mathbf{B}(\mathbf{x}) = \partial_x B_x(\mathbf{x}) + \partial_y B_y(\mathbf{x}). \quad (50)$$

The spatial derivatives of any field variable, namely, χ , are computed as

$$\nabla \chi(\mathbf{x}) = \frac{1}{c_s^2} \sum_i w_i \chi(\mathbf{x} + \mathbf{c}_i) \mathbf{c}_i. \quad (51)$$

The problem is governed by two dimensionless parameters: the Reynolds numbers, $Re = \frac{2\pi u_0}{\nu}$, and the magnetic Prandtl number, $Pr_m = \frac{\nu}{\eta}$. Consistently with De Rosis *et al.*,⁴⁹ a low Mach number equal to $Ma = \frac{u_0}{S_v c_s} \simeq 0.028$ is adopted in all the simulations, where S_v is a scaling factor allowing us to transform the velocity u_0 into LB units.⁴⁹

Our numerical campaign begins by simulating a scenario where $\nu = \eta = 0.02$, corresponding to a Reynolds number of $Re \simeq 628$. Tables I–III report the peak values of (i) the vorticity, $\zeta_{\max} = \max_x |\zeta(\mathbf{x})|$; (ii) the density of electric current, $j_{\max} = \max_x |j(\mathbf{x})|$;

TABLE I. Two-dimensional MHD vortex flow at $\nu = \eta = 0.02$: peak values of the vorticity at salient time instants and different grid resolutions by the present approach and other LBMs from De Rosis *et al.*,⁴⁹ together with findings from Dellar.³¹ [Reproduced with the permission from De Rosis *et al.*, Phys. Fluids 33, 035143 (2021). Copyright 2021 AIP Publishing. Reproduced with permission from P. J. Dellar, J. Comput. Phys. 179, 95 (2002). Copyright 2002 Elsevier.]

t	L	Dollar ³¹	BGK	MRT	CMS	SLBM	SSLBM
0.5	128	6.744	6.687	6.685	6.685	6.566	6.625
	256	6.754	6.738	6.737	6.737	6.719	6.722
	512	6.758	6.752	6.752	6.752	6.748	6.748
	1024	...	6.756	6.756	6.756	6.755	6.755
1.0	128	14.07	13.23	13.03	13.03	9.50	12.35
	256	14.16	13.94	13.92	13.92	12.67	13.64
	512	14.20	14.13	14.12	14.12	13.91	14.03
	1024	...	14.18	14.18	14.18	14.15	14.17

TABLE II. Two-dimensional MHD vortex flow at $\nu = \eta = 0.02$: peak values of the density of electric current at salient time instants and different grid resolutions by the present approach and other LBMs from De Rosis *et al.*,⁴⁹ together with findings from Dellar.³¹ [Reproduced with the permission from De Rosis *et al.*, Phys. Fluids 33, 035143 (2021). Copyright 2021 AIP Publishing. Reproduced with permission from P. J. Dellar, J. Comput. Phys. 179, 95 (2002). Copyright 2002 Elsevier.]

t	L	Dollar ³¹	BGK	MRT	CMS	SLBM	SSLBM
0.5	128	17.96	18.39	18.39	18.39	15.17	16.88
	256	18.20	18.28	18.29	18.29	17.48	17.88
	512	18.24	18.25	18.25	18.25	18.09	18.15
	1024	...	18.24	18.24	18.24	18.21	18.22
1.0	128	45.13	47.58	47.51	47.50	31.39	39.62
	256	46.30	46.93	46.92	46.92	41.41	44.53
	512	46.59	46.70	46.70	46.70	45.51	46.09
	1024	...	46.64	46.64	46.64	46.42	46.49

and (iii) the divergence of the magnetic field, $\max_x |\nabla \cdot \mathbf{B}(\mathbf{x})|$ normalized by b_0 . Two salient time instants are considered: $t = 0.5$ and 1. The grid resolution varies as $L = 128, 256$, and 512. Results indicate that the SSLBM increases the accuracy of the computations of both the velocity and magnetic fields with respect to the SLBM. This is particularly evident for the coarsest lattice, where the advantage is particularly prominent. We address this behavior to the lower numerical dissipation introduced by the present method with respect to the classical simplified strategy. Interestingly, the proposed scheme is also able to keep very low peak values of the divergence of the magnetic field, that is, 10^{-16} – 10^{-15} , that can be considered an excellent numerical approximation of the divergence-free condition.

The aggregate view in Fig. 1 clearly highlights the large discrepancy of the SLBM at the lowest grid resolution that is alleviated by the present SSLBM. Figure 2 shows the contour lines of the density of electric current and vorticity at representative time instants. In agreement with Refs. 31 and 49, thin layers with large currents and vorticities arise in the domain as the time advances.

Let us investigate further scenarios characterized by different Reynolds numbers Prandtl number equal to 1. This is achieved by varying the fluid kinematic viscosity as $\nu = \eta = 0.08, 0.04, 0.01$, and 0.05. All the runs are carried out by assuming $L = 1024$. Maxima of the dissipation rate, $\max_t [\epsilon(t)]$, are reported in Table IV for all the considered approaches. While the LBMs with evolution of populations show identical results, the SLBM differs from these, especially when more turbulent scenarios are involved. Interestingly, findings obtained by the SSLBM are closer to those provided by the BGK, MRT, and CMS LBMs. Again, this behavior should be addressed to the lower dissipation and subsequent superior accuracy properties of the proposed approach. Interestingly, the SSLBM demonstrates that the maximum value of $\epsilon(\max_t [\epsilon(t)])$ decreases of $\simeq 20\%$ when the viscosity reduces by a half, as observed in the seminal work by Orszag and Tang¹¹ and more recently in De Rosis *et al.*⁴⁹ For the sake of completeness, these findings are also plotted in Fig. 3. Figure 4 sketches the contour map of the density of electric current at salient time instants. As the Reynolds number increases, the peak values of this quantity appear localized in a sheet in the center of the domain. This sheet becomes progressively thinner and longer with Re , with its magnitude growing

TABLE III. Two-dimensional MHD vortex flow at $\nu = \eta = 0.02$: peak values of the divergence of the magnetic field normalized by b_0 at salient time instants and different grid resolutions by the present approach and other LBMs from by De Rosis *et al.*⁴⁹ together with findings from Dollar.³¹ [Reproduced from De Rosis *et al.*, Phys. Fluids 33, 035143 (2021). Copyright 2021 AIP Publishing. Reproduced with permission from P. J. Dollar, J. Comput. Phys. 179, 95 (2002). Copyright 2002 Elsevier.]

t	L	Dollar ³¹	BGK	MRT	CMS	SLBM	SSLBM
0.5	128	0.0939	3.69×10^{-6}	3.59×10^{-6}	3.61×10^{-6}	2.74×10^{-16}	9.39×10^{-16}
	256	0.0246	5.18×10^{-8}	5.24×10^{-8}	5.24×10^{-8}	7.00×10^{-16}	1.90×10^{-15}
	512	0.0062	2.04×10^{-9}	2.04×10^{-9}	2.04×10^{-9}	1.51×10^{-15}	3.58×10^{-15}
	1024	...	6.09×10^{-10}	6.09×10^{-10}	6.09×10^{-10}	2.97×10^{-15}	1.77×10^{-15}
1.0	128	0.5642	3.44×10^{-5}	3.13×10^{-5}	3.15×10^{-5}	3.88×10^{-16}	9.21×10^{-16}
	256	0.1611	7.98×10^{-7}	7.89×10^{-7}	7.89×10^{-7}	7.00×10^{-16}	1.68×10^{-15}
	512	0.0415	6.20×10^{-8}	6.19×10^{-8}	6.19×10^{-8}	1.60×10^{-15}	3.27×10^{-15}
	1024	...	2.11×10^{-8}	2.11×10^{-8}	2.11×10^{-8}	3.64×10^{-15}	2.28×10^{-15}

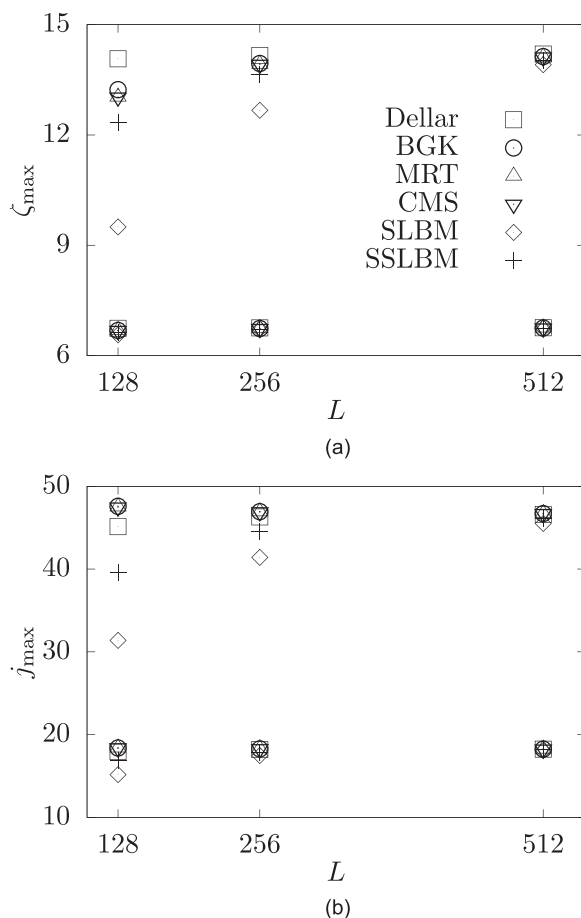


FIG. 1. Two-dimensional MHD vortex flow at $\nu = \eta = 0.02$: aggregate view of (a) peak values of the vorticity (ζ_{\max}) in Table I and (b) peak values of the density of electric current (j_{\max}) in Table II. Findings are obtained from Dollar³¹ (squares), BGK LBM (circles), MRT LBM (triangles), CMS-based LBM (inverted triangles), two-stage simplified LBM (diamonds), and present one-stage simplified LBM (crosses) [Reproduced with the permission from De Rosis *et al.*, Phys. Fluids 33, 035143 (2021). Copyright 2021 AIP Publishing. Reproduced with the permission from P. J. Dollar, J. Comput. Phys. 179, 95 (2002). Copyright 2002 Elsevier].

too. Moreover, it tends to dissipate earlier in time for larger values of the viscosity. A vis-à-vis comparison with the results reported in Fig. 8 of the work by De Rosis *et al.*⁴⁹ clearly highlights an optimal consistency of the proposed SSLBM with the schemes based on the evolution of populations.

Furthermore, let us consider the following four configurations with variable Re and Pr_m : (a) $\nu = \eta = 0.02$; (b) $\nu = 0.04$ and $\eta = 0.02$; (c) $\nu = 0.02$ and $\eta = 0.04$; (d) $\nu = \eta = 0.04$. Table V reports the peak values of the density of electric current at salient time instants obtained the MRT LBM, $j_{\max,\text{MRT}}$, together with the absolute discrepancies of the other LBMs with respect to it. These discrepancies are computed as

$$\begin{aligned} d_{\text{BGK}} &= |j_{\max,\text{MRT}} - j_{\max,\text{BGK}}|, \\ d_{\text{CMS}} &= |j_{\max,\text{MRT}} - j_{\max,\text{CMS}}|, \\ d_{\text{SLBM}} &= |j_{\max,\text{MRT}} - j_{\max,\text{SLBM}}|, \\ d_{\text{SSLBM}} &= |j_{\max,\text{MRT}} - j_{\max,\text{SSLBM}}|, \end{aligned} \quad (52)$$

where $j_{\max,\text{BGK}}$, $j_{\max,\text{SLBM}}$, $j_{\max,\text{SSLBM}}$ are the peak values of the density of electric current computed by BGK, SLBM, and SSLBM, respectively, and $d_{\max,\text{BGK}}$, $d_{\max,\text{SLBM}}$, $d_{\max,\text{SSLBM}}$ are the corresponding absolute deviations from the values provided by the MRT LBL. From this table, one can immediately appreciate that results provided by the CMS are identical to those form the MRT. The BGK LBM exhibits very small deviations. The SLBM shows the highest discrepancies, which are considerably alleviated by the SSLBM. Independently from the configuration, one can appreciate that the SSLBM generates results, which are in closer agreement with those obtained by LBMs with the evolution of distribution functions (BGK, MRT, and CMS) than obtained by SLBM.

In the following, configuration (a) is adopted to compare the run time of all the adopted schemes. Specifically, Fig. 5 depicts the central processing unit (CPU) time taken to simulate the range $t \in [0 : 1]$ with different grid resolutions. MRT, CMS, and BGK LBMs are observed to take the least CPU time, with little variation between them. SSLBM is observed to be the slowest. Its overhead in time is due to additional arithmetic operations per lattice point as described in Sec. II. Nevertheless, the accuracy improvements over the SLBM are self-evident and will be further demonstrated in Sec. III B in the application to three-dimensional scenarios. Furthermore, it is relevant to

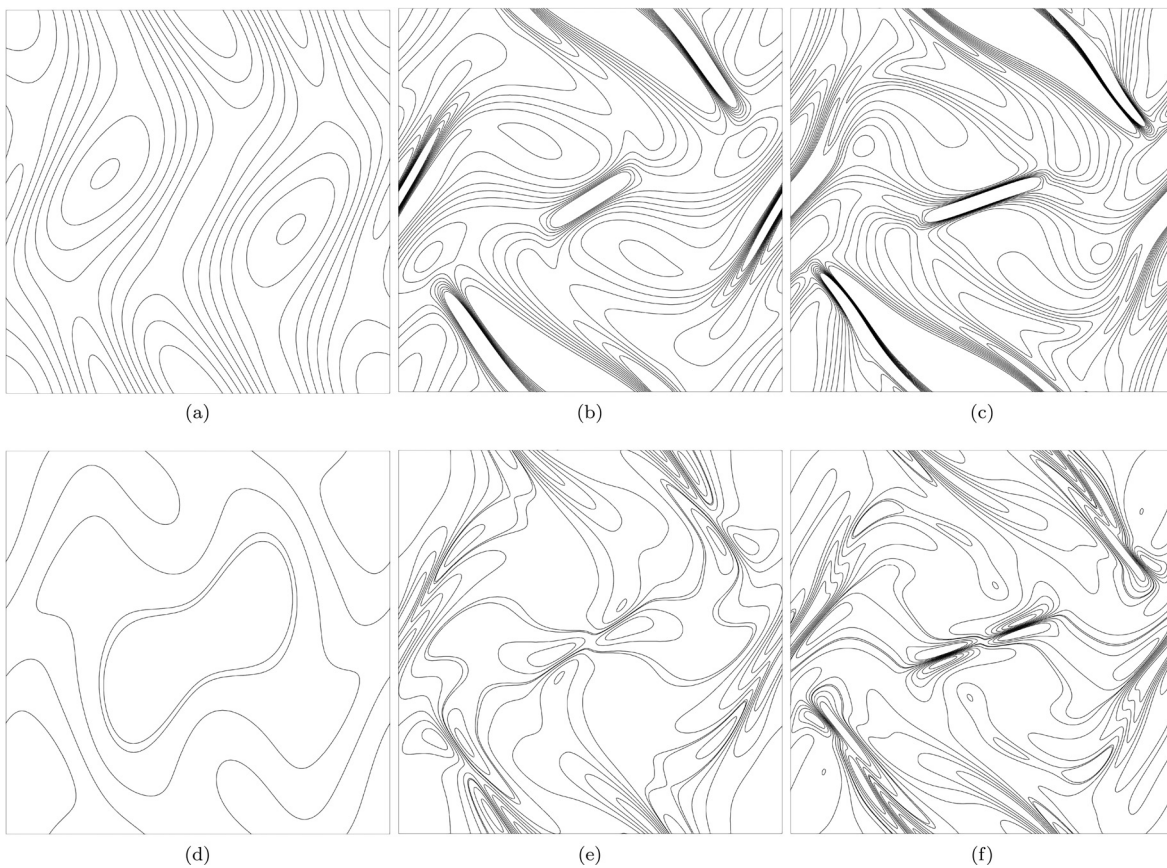


FIG. 2. Two-dimensional MHD vortex flow at $\nu = \eta = 0.02$: contour lines of the density of electric current at (a) $t = 0.2$, (b) 0.6 , (c) 0.85 and vorticity at (d) $t = 0.2$, (e) 0.6 , (f) 0.85 .

27 September 2024 08:56:46

note that this cost is expected to be more than offset by computational efficiencies brought by a reduced numerical stencil size when employed on memory-bound computer hardware such as graphics process unit (GPU) processing (see Mawson and Revell⁵⁹).

B. Three-dimensional simulations

Let us test the ability of the proposed scheme to simulate a three-dimensional scenario by considering the MHD vortex flow developing

TABLE IV. Two-dimensional MHD vortex flow at $\text{Pr}_m = 1$ and variable Re : maxima of the dissipation rate ϵ ($\times 10$) obtained by the present approach and other LBMs in De Rosis *et al.*⁴⁹ [Reproduced with the permission from De Rosis *et al.*, Phys. Fluids 33, 035143 (2021). Copyright 2021 AIP Publishing.]

ν	BGK	MRT	CMS	SLBM	SSLBM
0.08	16.131	16.131	16.131	16.134	16.132
0.04	13.424	13.424	13.424	13.418	13.423
0.02	10.758	10.758	10.758	10.736	10.751
0.01	8.318	8.318	8.318	8.253	8.300
0.005	6.280	6.280	6.280	6.106	6.246

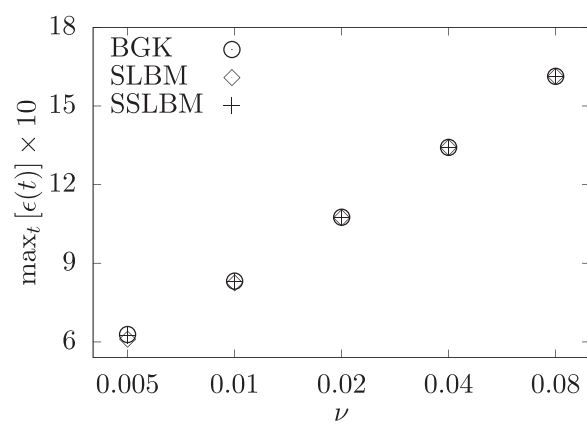


FIG. 3. Two-dimensional MHD vortex flow at $\text{Pr}_m = 1$ and variable Re : plot of the maxima of the dissipation rate ($\max_t [\epsilon(t)] \times 10$) reported in Table IV. Findings are obtained from BGK LBM (circles), two-stage simplified LBM (diamonds), and present one-stage simplified LBM (crosses) [Reproduced with the permission from De Rosis *et al.*, Phys. Fluids 33, 035143 (2021). Copyright 2021 AIP Publishing.]

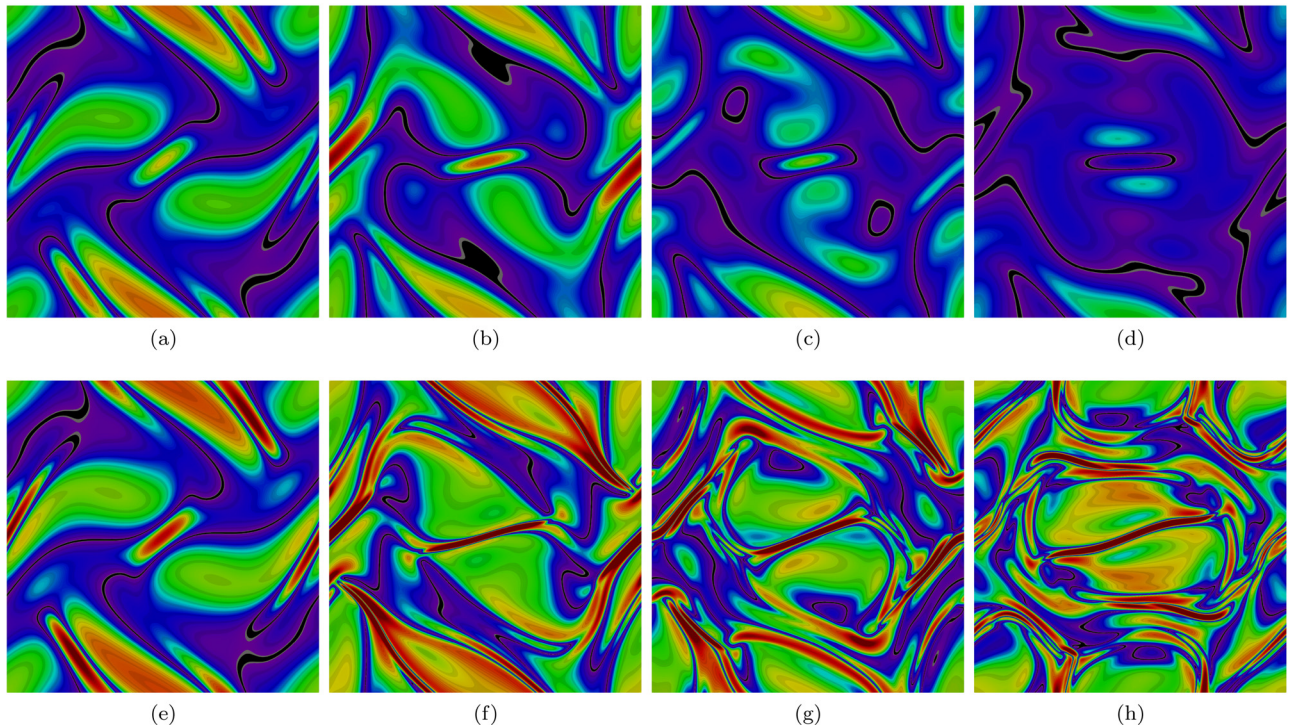


FIG. 4. Two-dimensional MHD vortex flow at $\text{Pr}_m = 1$ and variable Re : map of the density of electric current at salient time instants for different values of ν . $\nu = 0.08$ at (a) $t = 0.5$, (b) 1, (c) 1.5, and (d) 2. $\nu = 0.005$ at (e) $t = 0.5$, (f) 1, (g) 1.5, and (h) 2. Color map ranges from 0 (black) to 20 (dark red).

TABLE V. Two-dimensional MHD vortex flow at variable Re and Pr_m : peak value of the density of electric current $j_{\max, \text{MRT}}$ at salient time instants by the MRT together with the absolute discrepancies of the other LBMs in De Rosis *et al.*⁴⁹ with respect to it under different configurations. [Reproduced with the permission from De Rosis *et al.*, Phys. Fluids **33**, 035143 (2021). Copyright 2021 AIP Publishing.]

t	Conf.	MRT	d_{CMS}	d_{BGK}	d_{SLBM}	d_{SSLBM}
0.5	(a)	18.242	0	0	0.030	0.024
	(b)	17.655	0	0.001	0.027	0.023
	(c)	14.746	0	0.001	0.017	0.014
	(d)	14.363	0	0.001	0.015	0.013
1	(a)	46.638	0	0.002	0.218	0.144
	(b)	41.320	0.001	0.004	0.265	0.114
	(c)	34.340	0	0.002	0.079	0.051
	(d)	31.413	0	0.001	0.061	0.042
1.5	(a)	35.745	0	0.006	0.235	0.106
	(b)	35.159	0	0.005	0.209	0.095
	(c)	17.855	0	0.003	0.036	0.028
	(d)	17.665	0	0.002	0.045	0.027
2	(a)	24.970	0	0.007	0.159	0.051
	(b)	26.670	0	0.005	0.153	0.049
	(c)	9.871	0	0.002	0.022	0.010
	(d)	10.847	0	0.002	0.023	0.011

in a cubic periodic box of volume $2\pi \times 2\pi \times 2\pi$ with the initial conditions defined according to Mininni *et al.*,¹⁵ that is,

$$\begin{aligned} \mathbf{u}(\mathbf{x}, t=0) &= u_0[2 \sin y, 2 \sin x, 0], \\ \mathbf{B}(\mathbf{x}, t=0) &= 0.8b_0[-2 \sin 2y + \sin z, 2 \sin x + \sin z, \sin x + \sin y], \end{aligned} \quad (53)$$

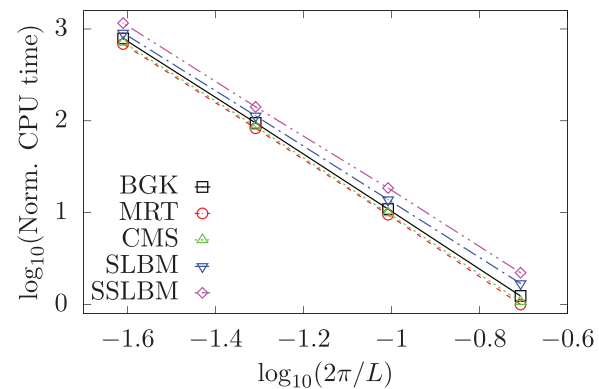


FIG. 5. CPU time (normalized by the minimum value corresponding to the fastest run) against grid resolution $2\pi/L$ involved by different schemes: BGK (black solid line with squares), raw-moments-based (MRT, red dashed line with circles), central-moments-based (CMS, green dotted line with triangles), two-stage simplified LBM (SLBM, blue dash-dotted line with inverted triangles), and single-stage simplified LBM (SSLBM, magenta dash-dot-dotted line with diamonds).

with $u_0 = b_0 = 1$. Similarly to the two-dimensional case, here the flow is characterized by intermittent small-scale structures. However, the topology of the reconnection of the magnetic field is considerably more complicated in three dimensions; hence, the simulation of this problem represents a tougher problem.⁶⁰ In three dimensions, the density of electric current vector has three non-zero components, that is, $\mathbf{j} = \nabla \times \mathbf{B} = [j_x, j_y, j_z]$, which are defined as

$$\begin{aligned} j_x &= \partial_y B_z - \partial_z B_y, \\ j_y &= \partial_z B_x - \partial_x B_z, \\ j_z &= \partial_x B_y - \partial_y B_x. \end{aligned} \quad (54)$$

We can compute the peak value of the density of the electric current as $j_{\max} = \max_x |j(x)|$, where $|j| = \sqrt{j_x^2 + j_y^2 + j_z^2}$. Notice that the divergence of the magnetic field is computed as $\nabla \cdot \mathbf{B} = \partial_x B_x + \partial_y B_y + \partial_z B_z$ in three dimensions.

Let us consider a scenario where $\nu = \eta = 0.057$. The box is represented by 128^3 lattice points, and the Mach number of the simulations is $\text{Ma} = \frac{u_0}{S\nu} \frac{1}{c_s} \simeq 0.00407$. The D3Q19 lattice discretization is adopted. In Fig. 6, the time evolution of j_{\max} is depicted. Findings obtained by the present SSLBM are plotted together with the results obtained by a high-resolution pseudo-spectral analysis (PS) and those coming from SLBM and BGK runs. The latter is characterized by large-amplitude oscillations in the earliest stage ($t < 0.1$) of the simulations, which vanish rapidly and do not deteriorate the solution in the later stage. Interestingly, one can immediately observe that the SSLBM generates results, which are considerably closer to the reference pseudo-spectral solution rather than those achieved by the SLBM. When $t > 0.45$, the SLBM produces a solution that largely underestimates j_{\max} . This is particularly evident with respect to the maximum value. Conversely, the SSLBM is able to capture well the knee at $t \sim 0.95$ and the subsequent bell-shaped behavior.

This is further quantified in Table VI, where the discrepancy of the BGK, SSLBM, and SLBM with respect to the pseudo-spectral values is computed as

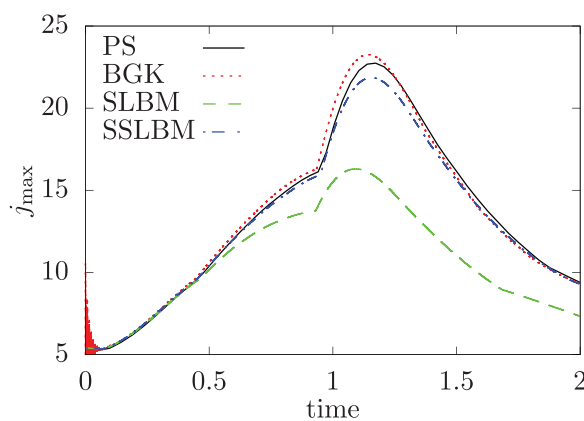


FIG. 6. Three-dimensional MHD vortex flow: time evolution of the peak value of the density of electric current obtained by (i) a high-resolution pseudo-spectral analysis (PS, black solid line, courtesy of Dr. R. Chahine⁵¹), (ii) the BGK LBM (red dashed line), (iii) the two-stage SLBM (green dashed dotted line), and (iv) the present one-stage method (blue dash-dotted line).

TABLE VI. Three-dimensional MHD vortex flow: maximum of the peak values of the density of the electric current by a high-resolution pseudo-spectral analysis, the BGK LBM, the two-stage SLBM, and the present one-stage method and relative discrepancies.

PS	BGK	SLBM	SSLBM	$\varepsilon_{\text{BGK}} [\%]$	$\varepsilon_{\text{S}} [\%]$	$\varepsilon_{\text{SS}} [\%]$
22.7439	23.2562	16.3016	21.8528	2.25	28.33	3.92

$$\begin{aligned} \varepsilon_{\text{BGK}} &= \frac{|\max_t [j_{\max, \text{PS}}(t)] - \max_t [j_{\max, \text{BGK}}(t)]|}{|\max_t [j_{\max, \text{PS}}(t)]|} \times 100, \\ \varepsilon_{\text{S}} &= \frac{|\max_t [j_{\max, \text{PS}}(t)] - \max_t [j_{\max, \text{S}}(t)]|}{|\max_t [j_{\max, \text{PS}}(t)]|} \times 100, \\ \varepsilon_{\text{SS}} &= \frac{|\max_t [j_{\max, \text{PS}}(t)] - \max_t [j_{\max, \text{SS}}(t)]|}{|\max_t [j_{\max, \text{PS}}(t)]|} \times 100, \end{aligned} \quad (55)$$

where \max_t denotes the maximum value of the desired quantity over the considered time range, and $j_{\max, \text{PS}}$, $j_{\max, \text{BGK}}$, $j_{\max, \text{S}}$, and $j_{\max, \text{SS}}$ are the time-dependent peak values of the density of the electric current obtained by the pseudo-spectral analysis,⁶¹ the BGK LBM, the simplified lattice Boltzmann method, and the present scheme, respectively. From this table, it is possible to appreciate that the error obtained by the present method is about seven times lower than the one made by the classical two-step simplified approach. Moreover, it is just 1.7 times larger than the one achieved by the BGK run. Present errors are computed by discretizing each side of the domain by 128 points, as mentioned. Such an apparently coarse grid resolution has been chosen as a trade-off between accuracy and computational cost. Nevertheless, the usage of finer grids will certainly reduce the mismatch with respect to the pseudo-spectral reference values.

In Fig. 7, the contour plot of the magnitude of the density of electric current is depicted at representative time instants. Thin sheets characterized by strong currents arise in the range $t \in [1 : 1.5]$ that is consistent with the high values of $|j|$ reported in Fig. 6. Interestingly, regions with high currents correspond to vanishing values of the magnetic field (see Fig. 8). These findings corroborate the results shown in Refs. 15 and 32 in two and three dimensions, respectively, as well as the observations in the work by De Rosis,⁶² where a central-moments-based collision operator was adopted. Notably, the transition to turbulence of the Orszag-Tang vortex has been recently investigated by direct numerical simulations in a recent work by Jadhav and Chandy.⁶³

Eventually, it is worth to underline that both the adopted LBMs satisfy very well the condition $\nabla \cdot \mathbf{B} = 0$. In fact, our computations are characterized by values of this quantity of order 10^{-16} , which is an excellent numerical approximation.

With respect to other efforts, here we elucidate the role of the magnetic Prandtl number in the three-dimensional vortex flow. Specifically, we rerun the same simulation by varying Pr_m as $\text{Pr}_m = 0.5, 1, 2$. In Fig. 9, the time evolution of the peak value of the density of electric current is reported for these scenarios. One can immediately observe that j_{\max} tends to grow with Pr_m . We address this behavior to the fact that scenarios characterized by higher value of Pr_m correspond to lower values of η (i.e., ν is kept fixed). Therefore, the diffusion coefficient of the magnetic field reduces and more magnetically turbulent scenarios are achieved. These findings are confirmed in

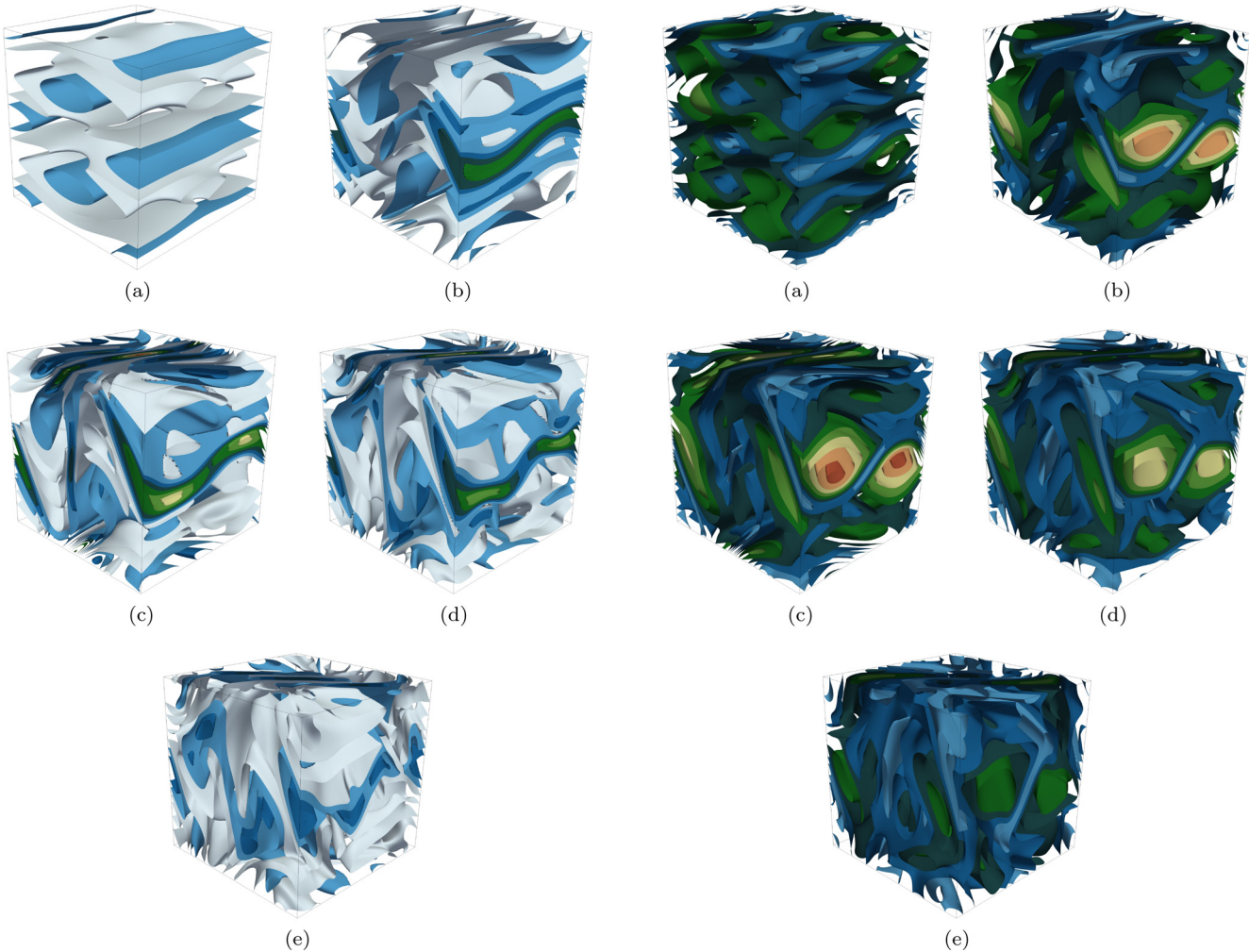


FIG. 7. Three-dimensional MHD vortex flow: map of the magnitude of the density of electric current at representative time instants: (a) $t = 0$, (b) 0.5, (c) 1.0, (d) 1.5, and (e) 2.0. Color map ranges from 2 (ice) to 20 (red).

Fig. 10, where the time evolution of the magnetic, kinetic, and total energies is depicted. While E_k and E tend to monotonically decrease, E_m undergoes larger variations due to an exchange of energy, which corroborates the observations in two-dimensional simulations.^{11,32,49}

IV. CONCLUSIONS

In a very recent effort,⁴⁹ the simplified LBM has been shown as able to enforce the divergence-free condition $\nabla \cdot \mathbf{B} = 0$ in an excellent manner. However, it has demonstrated poorer accuracy if compared to the adoption of the BGK and MRT collision operators. In this paper, we presented, tested, and validated a simplified lattice Boltzmann method for two- and three-dimensional magnetohydrodynamic flows with improved accuracy. Differently from its classical formulation, here the two-stage procedure is replaced by a one-stage one. While keeping the same excellent performance of the SLBM in the satisfaction of the divergence-free condition of the magnetic field, we

FIG. 8. Three-dimensional MHD vortex flow: map of the magnitude of the magnetic field at representative time instants: (a) $t = 0$, (b) 0.5, (c) 1.0, (d) 1.5, and (e) 2.0. Color map ranges from 0 (ice) to 5 (red).

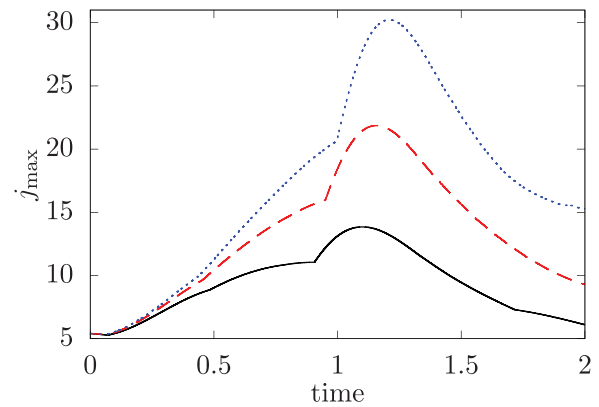


FIG. 9. Three-dimensional MHD vortex flow: time evolution of the peak value of the density of electric current at $Pr_m = 0.5$ (black solid line), 1 (red dashed line), and 2 (blue dotted line).

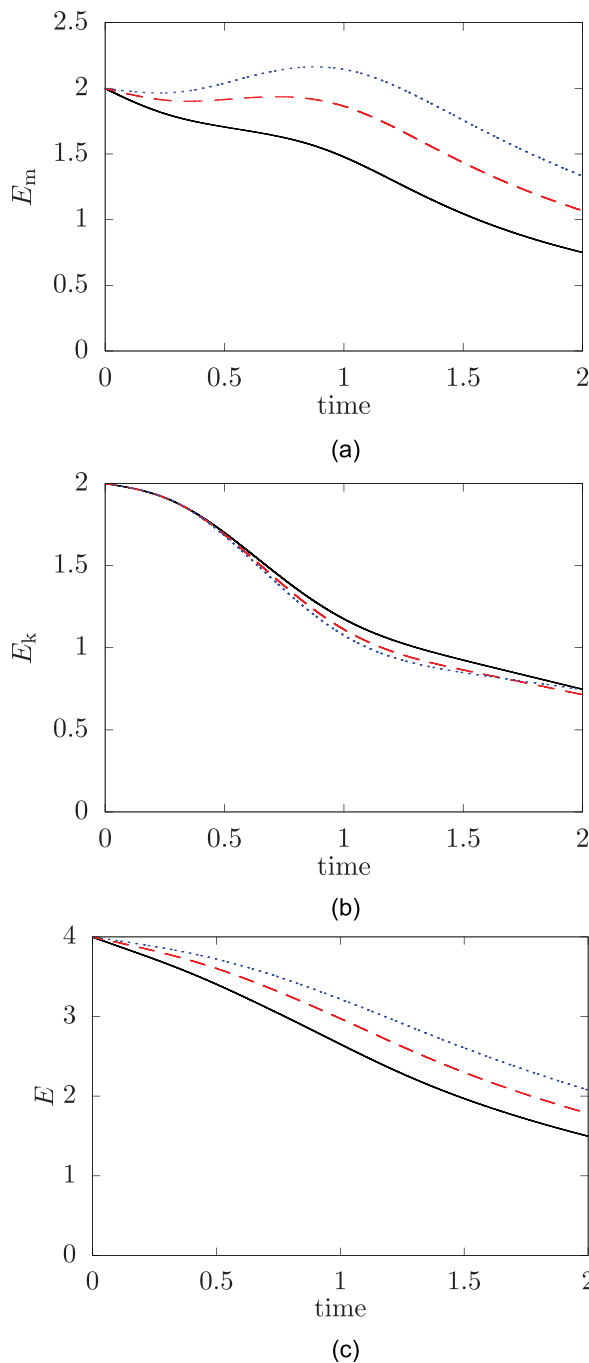


FIG. 10. Three-dimensional MHD vortex flow: time evolution of the magnetic, kinetic, and total energies at $\text{Pr}_m = 0.5$ (black solid line), 1 (red dashed line), and 2 (blue dotted line).

demonstrated that the SSLBM is characterized by a superior accuracy. This is particularly evident when three-dimensional scenarios are considered, where the dissipation properties of the SLBM dominate excessively the flow physics.

In summary, we believe that the SSLBM is an excellent candidate to perform numerical simulations of magnetohydrodynamic flows for the following reasons:

- $\nabla \cdot \mathbf{B} = 0$ excellently satisfied, with values that are several orders of magnitude lower than those achieved by LBMs with the evolution of populations;
- low amount of required virtual memory, allowing us to use one tenth of the one required by LBMs with the evolution of populations;
- superior accuracy with respect to findings obtained by the SLBM.

In a future work, we aim at performing systematic comparisons of the statistical properties of MHD turbulence.^{64–66}

SUPPLEMENTARY MATERIAL

See the [supplementary material](#) for in order to help the reader to reproduce our results, we add in the [supplementary material](#) a C++ programs, SSLBM.cpp, which implement the present one-stage models. It allows the interested reader to simulate the two-dimensional MHD flows discussed in Sec. III. The code used in this work is included in the [supplementary material](#), along with a README file containing details and compilation instructions needed to run. In this way, the interested reader is able to reproduce the results in this paper.

ACKNOWLEDGMENTS

A.D.R. would like to thank Dr. E. Lévéque and Dr. W. J. T. Bos for their help in understanding the physics of magnetohydrodynamic turbulence.

A.D.R. is also grateful to Dr. R. Chahine who kindly provided the pseudo-spectral data plotted in Fig. 6.

DATA AVAILABILITY

The data that support the findings of this study are available from the corresponding author upon reasonable request.

REFERENCES

- ¹H. Alfvén, “Existence of electromagnetic-hydrodynamic waves,” *Nature* **150**, 405–406 (1942).
- ²J. Zhong, M. Yi, and H. H. Bau, “Magneto hydrodynamic (MHD) pump fabricated with ceramic tapes,” *Sens. Actuators, A* **96**, 59–66 (2002).
- ³R. Zhao, X. Dou, D. Zhang, and J. Huang, “Numerical study of the magnetohydrodynamic flow instability and its effect on energy conversion in the annular linear induction pump,” *Phys. Fluids* **33**, 067125 (2021).
- ⁴R. Ellahi, A. Zeeshan, N. Shehzad, and S. Z. Alamri, “Structural impact of Kerosene-Al₂O₃ nanoliquid on MHD Poiseuille flow with variable thermal conductivity: Application of cooling process,” *J. Mol. Liquids* **264**, 607–615 (2018).
- ⁵M. Vandas, D. Odstrčil, and S. Watari, “Three-dimensional MHD simulation of a loop-like magnetic cloud in the solar wind,” *J. Geophys. Res.* **107**, SSH-2-1, <https://doi.org/10.1029/2001JA005068> (2002).
- ⁶V. Nakariakov, A. Inglis, I. Zimovets, C. Foullon, E. Verwiche, R. Sych, and I. Myagkova, “Oscillatory processes in solar flares,” *Plasma Phys. Controlled Fusion* **52**, 124009 (2010).
- ⁷S. Miralles, G. Verhille, N. Plihon, and J.-F. Pinton, “The magnetic-distortion probe: Velocimetry in conducting fluids,” *Rev. Sci. Instrum.* **82**, 095112 (2011).
- ⁸G. Bousselini, M. Tanase, M. Moulin, and N. Plihon, “Flowrate measurements of conducting fluids in pipes using the magnetic distortion probe,” *Meas. Sci. Technol.* **29**, 025302 (2018).

- ⁹V. Sukhotskiy, K. Tawil, and E. Einarsson, "Printability regimes of pure metals using contactless magnetohydrodynamic drop-on-demand actuation," *Phys. Fluids* **33**, 053303 (2021).
- ¹⁰J. Hartmann and F. Lazarus, "Hg-dynamics II," in *Theory of Laminar Flow of Electrically Conductive Liquids in a Homogeneous Magnetic Field* (Det Kgl. Danske Videnskabernes Selskab, 1937), Vol. 15.
- ¹¹S. A. Orszag and C.-M. Tang, "Small-scale structure of two-dimensional magnetohydrodynamic turbulence," *J. Fluid Mech.* **90**, 129–143 (1979).
- ¹²H. Politano, A. Pouquet, and P. Sulem, "Inertial ranges and resistive instabilities in two-dimensional magnetohydrodynamic turbulence," *Phys. Fluids B* **1**, 2330–2339 (1989).
- ¹³D. Biskamp and E. Schwarz, "On two-dimensional magnetohydrodynamic turbulence," *Phys. Plasmas* **8**, 3282–3292 (2001).
- ¹⁴A. Alexakis, P. D. Mininni, and A. Pouquet, "Shell-to-shell energy transfer in magnetohydrodynamics. I. Steady state turbulence," *Phys. Rev. E* **72**, 046301 (2005).
- ¹⁵P. Mininni, A. Pouquet, and D. Montgomery, "Small-scale structures in three-dimensional magnetohydrodynamic turbulence," *Phys. Rev. Lett.* **97**, 244503 (2006).
- ¹⁶K. Schneider, S. Neffaa, and W. J. Bos, "A pseudo-spectral method with volume penalisation for magnetohydrodynamic turbulence in confined domains," *Comput. Phys. Commun.* **182**, 2–7 (2011).
- ¹⁷R. Benzi, S. Succi, and M. Vergassola, "The lattice Boltzmann equation: Theory and applications," *Phys. Rep.* **222**, 145–197 (1992).
- ¹⁸T. Krüger, H. Kusumaatmaja, A. Kuzmin, O. Shardt, G. Silva, and E. M. Viggen, *The Lattice Boltzmann Method: Principles and Practice* (Springer International Publishing, 2017).
- ¹⁹S. Succi, *The Lattice Boltzmann Equation: For Complex States of Flowing Matter* (Oxford University Press, 2018).
- ²⁰Z. Chen, C. Shu, Y. Wang, L. Yang, and D. Tan, "A simplified lattice Boltzmann method without evolution of distribution function," *Adv. Appl. Math. Mech.* **9**, 1–22 (2017).
- ²¹Z. Chen, C. Shu, and D. Tan, "Highly accurate simplified lattice Boltzmann method," *Phys. Fluids* **30**, 103605 (2018).
- ²²Z. Chen, C. Shu, and D. Tan, "Immersed boundary-simplified lattice Boltzmann method for incompressible viscous flows," *Phys. Fluids* **30**, 053601 (2018).
- ²³Z. Chen, C. Shu, and D. S. Tan, "The simplified lattice Boltzmann method on non-uniform meshes," *Commun. Comput. Phys.* **23**, 1131 (2018).
- ²⁴Z. Chen, C. Shu, and D. Tan, "High-order simplified thermal lattice Boltzmann method for incompressible thermal flows," *Int. J. Heat Mass Transfer* **127**, 1–16 (2018).
- ²⁵Z. Chen, C. Shu, D. Tan, and C. Wu, "On improvements of simplified and highly stable lattice Boltzmann method: Formulations, boundary treatment, and stability analysis," *Int. J. Numer. Methods Fluids* **87**, 161–179 (2018).
- ²⁶Z. Chen and C. Shu, "On numerical diffusion of simplified lattice Boltzmann method," *Int. J. Numer. Methods Fluids* **92**, 1198 (2020).
- ²⁷Z. Chen, C. Shu, L. Yang, X. Zhao, and N. Liu, "Immersed boundary-simplified thermal lattice Boltzmann method for incompressible thermal flows," *Phys. Fluids* **32**, 013605 (2020).
- ²⁸S. Succi, M. Vergassola, and R. Benzi, "Lattice Boltzmann scheme for two-dimensional magnetohydrodynamics," *Phys. Rev. A* **43**, 4521 (1991).
- ²⁹S. Chen, H. Chen, D. Martnez, and W. Matthaeus, "Lattice Boltzmann model for simulation of magnetohydrodynamics," *Phys. Rev. Lett.* **67**, 3776 (1991).
- ³⁰D. O. Martínez, S. Chen, and W. H. Matthaeus, "Lattice Boltzmann magnetohydrodynamics," *Phys. Plasmas* **1**, 1850–1867 (1994).
- ³¹P. J. Dellar, "Lattice kinetic schemes for magnetohydrodynamics," *J. Comput. Phys.* **179**, 95–126 (2002).
- ³²A. De Rosis, E. Lévéque, and R. Chahine, "Advanced lattice Boltzmann scheme for high-Reynolds-number magneto-hydrodynamic flows," *J. Turbul.* **19**, 446–462 (2018).
- ³³P. Bhatnagar, E. Gross, and M. Krook, "A model for collision processes in gases. I. Small amplitude processes in charged and neutral one-component systems," *Phys. Rev.* **94**, 511 (1954).
- ³⁴P. J. Dellar, "Nonhydrodynamic modes and a priori construction of shallow water lattice Boltzmann equations," *Phys. Rev. E* **65**, 036309 (2002).
- ³⁵P. J. Dellar, "Non-hydrodynamic modes and general equations of state in lattice Boltzmann equations," *Physica A* **362**, 132–138 (2006).
- ³⁶J. Latt and B. Chopard, "Lattice Boltzmann method with regularized pre-collision distribution functions," *Math. Comput. Simul.* **72**, 165–168 (2006).
- ³⁷R. Adhikari and S. Succi, "Duality in matrix lattice Boltzmann models," *Phys. Rev. E* **78**, 066701 (2008).
- ³⁸G. Wissocq, P. Sagaut, and J.-F. Boussuge, "An extended spectral analysis of the lattice Boltzmann method: Modal interactions and stability issues," *J. Comput. Phys.* **380**, 311–333 (2019).
- ³⁹O. Malaspinas, "Increasing stability and accuracy of the lattice Boltzmann scheme: Recursivity and regularization," [arXiv:1505.06900](https://arxiv.org/abs/1505.06900) (2015).
- ⁴⁰C. Coreixas, G. Wissocq, G. Puigt, J.-F. Boussuge, and P. Sagaut, "Recursive regularization step for high-order lattice Boltzmann methods," *Phys. Rev. E* **96**, 033306 (2017).
- ⁴¹A. De Rosis and K. H. Luo, "Role of higher-order Hermite polynomials in the central-moments-based lattice Boltzmann framework," *Phys. Rev. E* **99**, 013301 (2019).
- ⁴²A. De Rosis, "A central moments-based lattice Boltzmann scheme for shallow water equations," *Comput. Methods Appl. Mech. Eng.* **319**, 379–392 (2017).
- ⁴³A. De Rosis, "Preconditioned lattice Boltzmann method for steady flows: A noncascaded central-moments-based approach," *Phys. Rev. E* **96**, 063308 (2017).
- ⁴⁴A. De Rosis, R. Huang, and C. Coreixas, "Universal formulation of central-moments-based lattice Boltzmann method with external forcing for the simulation of multiphysics phenomena," *Phys. Fluids* **31**, 117102 (2019).
- ⁴⁵M. B. Asadi, A. De Rosis, and S. Zendehboudi, "Central-moments-based lattice Boltzmann for associating fluids: A new integrated approach," *J. Phys. Chem. B* **124**, 2900–2913 (2020).
- ⁴⁶A. De Rosis and A. Tafuni, "A phase-field lattice Boltzmann method for the solution of water-entry and water-exit problems," *Comput.-Aided Civ. Infrastruct. Eng.* (published online) (2020).
- ⁴⁷S. Saito, A. De Rosis, L. Fei, K. H. Luo, K.-I. Ebihara, A. Kaneko, and Y. Abe, "Lattice Boltzmann modeling and simulation of forced-convection boiling on a cylinder," *Phys. Fluids* **33**, 023307 (2021).
- ⁴⁸A. De Rosis and E. Enan, "A three-dimensional phase-field lattice Boltzmann method for incompressible two-components flows," *Phys. Fluids* **33**, 043315 (2021).
- ⁴⁹A. De Rosis, J. Al-Adham, H. Al-Ali, and R. Meng, "Double-D2Q9 lattice Boltzmann models with extended equilibrium for two-dimensional magnetohydrodynamic flows," *Phys. Fluids* **33**, 035143 (2021).
- ⁵⁰L. Vahala, G. Vahala, and J. Yepez, "Lattice Boltzmann and quantum lattice gas representations of one-dimensional magnetohydrodynamic turbulence," *Phys. Lett. A* **306**, 227–234 (2003).
- ⁵¹G. Vahala, B. Keating, M. Soe, J. Yepez, L. Vahala, J. Carter, and S. Ziegeler, "MHD turbulence studies using lattice Boltzmann algorithms," *Commun. Comput. Phys.* **4**, 624–646 (2008), http://global-sci.org/intro/article_detail/cicp/7808.html.
- ⁵²C. Flint and G. Vahala, "A large eddy lattice Boltzmann simulation of magnetohydrodynamic turbulence," *Phys. Lett. A* **382**, 405–411 (2018).
- ⁵³C. Flint and G. Vahala, "A partial entropic lattice Boltzmann MHD simulation of the Orszag–Tang vortex," *Radiat. Eff. Defects Solids* **173**, 55–65 (2018).
- ⁵⁴C. Flint, G. Vahala, L. Vahala, and M. Soe, "A 9-bit multiple relaxation lattice Boltzmann magnetohydrodynamic algorithm for 2D turbulence," *Comput. Math. Appl.* **72**, 394–403 (2016).
- ⁵⁵L. Vienne and E. Lévéque, "Recursive finite-difference lattice Boltzmann schemes," *Comput. Math. Appl.* **96**, 95 (2021).
- ⁵⁶A. Delgado-Gutiérrez, P. Marzocca, D. Cárdenas, and O. Probst, "A single-step and simplified graphics processing unit lattice Boltzmann method for high turbulent flows," *Int. J. Numer. Methods Fluids* **93**, 2339 (2021).
- ⁵⁷C. Coreixas, B. Chopard, and J. Latt, "Comprehensive comparison of collision models in the lattice Boltzmann framework: Theoretical investigations," *Phys. Rev. E* **100**, 033305 (2019).
- ⁵⁸I. Karlin and P. Asinari, "Factorization symmetry in the lattice Boltzmann method," *Physica A* **389**, 1530–1548 (2010).

- ⁵⁹M. J. Mawson and A. J. Revell, "Memory transfer optimization for a lattice Boltzmann solver on Kepler architecture nVidia GPUs," *Comput. Phys. Commun.* **185**, 2566–2574 (2014).
- ⁶⁰J. M. Greene, "Geometrical properties of three-dimensional reconnecting magnetic fields with nulls," *J. Geophys. Res.* **93**, 8583–8590, <https://doi.org/10.1029/JA093iA08p08583> (1988).
- ⁶¹R. Chahine and W. J. T. Bos, "On the role and value of β in incompressible MHD simulations," *Phys. Plasmas* **25**, 042115 (2018).
- ⁶²A. De Rosis, "Nonorthogonal central-moments-based lattice Boltzmann scheme in three dimensions," *Phys. Rev. E* **95**, 013310 (2017).
- ⁶³K. Jadhav and A. J. Chandy, "Analysis of energy transfer through direct numerical simulations of magnetohydrodynamic Orszag–Tang vortex," *Phys. Fluids* **33**, 065112 (2021).
- ⁶⁴D. Banerjee and R. Pandit, "Two-dimensional magnetohydrodynamic turbulence with large and small energy-injection length scales," *Phys. Fluids* **31**, 065111 (2019).
- ⁶⁵A. Azulay, B. Mikhailovich, A. Levy, and A. Yakhot, "On turbulence measurement in rotating magnetic field-driven flow," *Phys. Fluids* **32**, 105121 (2020).
- ⁶⁶D. Viganò, R. Aguilera-Miret, and C. Palenzuela, "Extension of the subgrid-scale gradient model for compressible magnetohydrodynamics turbulent instabilities," *Phys. Fluids* **31**, 105102 (2019).